Effect of external heat loss on the propagation and quenching of flames in small heat-recirculating tubes

George P. Gauthier, and Jeffrey M. Bergthorson

Department of Mechanical Engineering, McGill University, Montréal, Quebec, Canada, H3A 0C3.

Abstract

This study investigates the effect of external heat loss on the slow propagation of strongly-burning flames inside narrow heat-recirculating tubes. The system is studied using a two-dimensional numerical model for reactive flow, including conjugate heat transfer, over a range of tube diameters spanning the micro- and the meso-scale. Increasing external heat loss decreases the propagation speed of the slowly-propagating flames, leading to a transition from upstream to downstream propagation, until a heat loss limit is reached. Flames in micro-scale tubes are subjected to an extinction limit, while flames in larger diameter tubes, in the meso-scale range, are subjected to a blowout limit. While the absolute value of the external convective heat loss coefficient at the extinction/blowout limit increases with diameter, the dimensionless volumetric heat loss coefficient decreases with an increase in diameter until an approximately constant value, for the studied conditions, is reached at the blowout limit in the mesoscale range. Discrepancies in the predicted trends of 1-D and 2-D models indicate that 2-D effects play a significant role at larger diameters, not only at the meso-scale, but also in the upper-range of the micro-scale. These 2-D effects, associated with changes in flame shape that allow an increase in burning surface area, are seen to promote stability of the system. Results have implications on the choice of tube diameter to be used in the design of a stable burner optimized for heat transfer to an external heat load. to promote stability of the system.

Keywords: Excess enthalpy, Heat recirculation, Micro-scale, Meso-scale, Extinction, Blowout

1. Introduction

Concerns about climate change and energy availability establish a need for alternative fuels to replace conventional fossil fuels. Under-utilized energy sources, such as biogas, syngas, landfill gas, and vented natural gas are promising alternatives [1–3]. Burner technologies are needed that can burn, directly, these mixtures of low heat content. Heat-recirculating burners, also referred to as excess-enthalpy burners [2], can increase the reactivity of mixtures, allowing the efficient burning of mixtures of low energy content [1].

Heat-recirculating burners rely on heat transfer via a solid structure to provide an alternate path, in addition to the gas path, for heat to reach unburnt reactants [2, 4]. In order for interfacial heat transfer between wall and fluid to be sufficient for the flame behavior to be influenced by heat recirculation, the surface-to-volume ratio of the gas stream should be large enough, leading to small characteristic dimensions of the flow channel [4]. These small dimensions are additionally advantageous for transferring heat from the reacting mixture to an external heat load. This load could be a power conversion system, such as an external-combustion engine [5–7] or a thermoelectric device [8, 9], whose efficiencies increase with heat source temperature [2, 9]. Maximization of heat source temperature requires heat transfer to occur close to the flame zone, such that there is a need for characterizing the effect of external heat loss on excess-enthalpy flames.

The effect of heat loss on conventional flames propagating in small flow passages has been studied extensively since the original work done by Davy [10]. Flames do not propagate through a flow passage when the gap size is smaller than the quenching distance. This phenomenon can be captured using a one-dimensional (1-D) modeling approach [11, 12] accounting for convective heat loss from the reacting fluid to a wall maintained at a constant temperature. Quenching is predicted to occur when the temperature-dependent heat release rates become too small to overcome heat loss across the flame [13]. Quenching diameter, D_q, is expected to be proportional to the flame thickness, δ_f. This leads to a Peclet number value at quenching, $\mathrm{Pe}_\mathrm{q} = D_\mathrm{q}/\delta_\mathrm{f}$, typically predicted to be of the order of 10 [14–16]. The 1-D thermal approach predicts the right length scale for quenching distance, on the order of a millimeter for hydrocarbon flames [17]. Quenching distance measurements of various mixtures are typically reported at room temperature [17]. When the fluid and wall temperatures are raised, the temperature dependent burning rates increase [18], allowing a reduction in quenching distance [18, 19]. It is therefore possible to obtain flames in tubes smaller than the conventional quenching diameter at elevated temperatures [18–20]. Detailed numerical and experimental studies on flame quenching in ducts have reported additional phenomena, such as multiple flame shapes [14, 21–23], partial quenching near the wall [15, 24], radical quenching [19, 25], and an influence of flow field on quenching distance [22, 24].

In studies investigating the quenching of conventional flames, it is assumed that the wall temperature stays unchanged. However, when the flame propagation velocity is made small, through a change in inflow velocity for example, the wall temperature can become significantly influenced by the flame heat release. This leads to heat-recirculation-dominated flame regimes, associated with slow flame propagation inside narrow tubes [26–32]. In order to model the dynamics and quenching limits of this system involving thermal coupling between the flame and the wall, temperature of the conducting wall needs to be resolved in addition to the fluid temperature field.

Previous studies have investigated the dynamics of flames in various configurations of heat-recirculating burners [29, 31, 33–39]. These burners allow for a large range of firing rates with flame speeds that can be more than ten times greater than the laminar flame speed predicted from inlet conditions [33, 38]. Heat loss is seen to reduce the range of permissible flow rates [35, 39]. At the low-end of this range, flames are subjected to an extinction-type limit, where bulk flame temperatures are reduced down to a point where heat release rates become too small to overcome heat loss [35, 36]. At the high-end of this range, flames are subjected to a blowout limit [33], where residence times inside the preheat zone become too small for the flame to stay coupled to the wall thermal profile [36].

Norton and Vlachos [36] have specifically investigated the influence of external heat loss on flames in small heat-recirculating channels using a 2-D elliptic model with conjugate heat transfer. It is found that there exists an optimum wall thermal conductivity maximizing burner stability; burner stability refers to the range of permissible values of external heat transfer coefficient. Channels of small width are more likely to sustain an extinction-type limit, while larger channels are more prone to a blowout-type limit. In a subsequent study by the same group [40], a 1-D model is used to evaluate burner stability over a wide range of channel widths. An optimal gap width, at which burner stability is maximized, is found for a particular set of conditions. However, in the 1-D model formulation used in that study, the flame structure is assumed to be flat, such that changes in flame shape are not captured.

In our previous study on heat-recirculating flames in narrow tubes [32], changes in flame shape are observed to become significant when tube diameter and inflow velocity are increased. This leads to highly curved flames for which heat recirculation is significantly reduced, and where burning rate enhancement is

mainly associated with an increase in flame burning area [32]. Flame-normal burning velocity at the surface of elongated flames remains close to the laminar burning velocity. Since these elongated excess-enthalpy flames have only been investigated at adiabatic conditions [32], or over a restricted range of conditions [36, 41], the impact of external heat loss is still unclear.

In this study, a two-dimensional model for reacting flow with conjugate heat transfer is used to accurately simulate the slow propagation of excess-enthalpy flames in narrow tubes, over a range of tube diameters spanning the micro- and the meso-scale. Heat loss conditions are varied in order to assess their influence on propagation of thermally-coupled flames, and to determine limits of operation. One-dimensional model predictions, which are typically used to model the behavior of this type of system [18, 28, 29, 31, 42, 43], are used as an hypothesis for the trends to be observed in the study. Qualitative discrepancies in model predictions are used to assess the influence of two-dimensional flame structure effects on the behavior of the system. Flame characteristics are examined to determine the mechanisms leading to heat loss limits in the system.

While heat loss is typically considered to be detrimental, leading to a reduction in available heat at the burner exit [37], this study considers heat loss as a useful phenomenon that allows high-temperature heat transfer to a heat load. This study aims at determining the maximum heat loading an excess-enthalpy flame can sustain, and to help determine which tube diameter is most advantageous for heat transfer to an external heat load; tube diameter being a critical parameter to be determined in the design of an efficient burner for power production. Only stable, strongly-burning flames are considered in this study as they provide the highest power density for power production.

2. Numerical formulation

The system of interest, shown in Fig. 1, consists of a tube of circular cross-section of finite wall thickness in which a flame propagates. This system is the same as the one used in [32], with the difference that the external tube surface is not adiabatic, but subjected to a convective heat loss to the surroundings. This simple geometry can be considered as a fundamental case that extends the classical study of flame quenching inside tubes to a system where heat recirculation occurs inside the tube wall. This study focuses on strongly-burning heat-recirculating flames [32] for which a typical temperature field is shown in shades of gray. The inflow velocity, referred to as S_{in}, corresponds to the mean velocity of the fully-developed parabolic velocity profile that exists upstream of the flame. S_{p} refers to the flame propagation velocity, which is expected to be small in the slowly propagating flame regime. S_{p} is positive when the flame is travelling upstream, and is negative when the flame is moving downstream. Burning velocity of the flame is denoted as S_{b}, and is the sum of inlet and propagation velocities. In this study, the ratio between wall thickness, t_{w}, and tube inner diameter, D, is kept constant, as shown in Fig. 1.

2.1. One-dimensional asymptotic model

While burning properties of conventional flames are influenced by flow conditions and heat loss conditions, heat-recirculating flames are also dependent on wall properties. This makes the parametric space of the problem larger than for a conventional laminar flame, rendering the mapping of solution space a considerable task [31]. One-dimensional asymptotic models have been proposed [18, 28, 29, 31, 42, 44] that can efficiently capture the various burning regimes occurring in heat-recirculating tubes. In these simplified models, fields are assumed to be uniform in the transverse or radial direction, and the interfacial heat transfer between gas and wall is captured using Newton's law of cooling. The 1-D governing equations are solved in the limit of

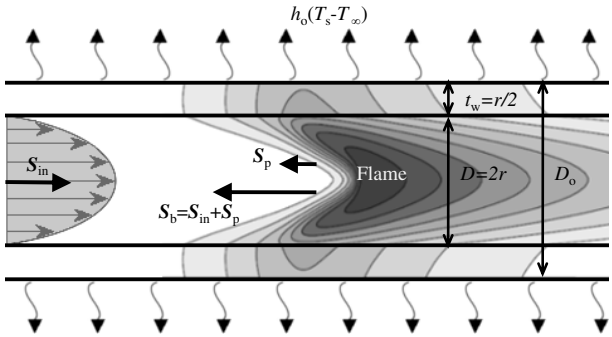

Figure 1: System of interest: tube of circular cross-section of inner diameter D, outer diameter D_o, and wall thickness t_w, in which a flame propagates. The external tube wall is subjected to convective heat loss to the surroundings. The incoming flow field is a fully-developed parabolic velocity profile of mean velocity S_{in}. The flame propagates at a speed S_p, and the burning velocity is denoted as S_b. Typical temperature contours are shown in shades of gray.

the flame sheet assumption, with constant properties and a simplified chemistry scheme consisting only of the deficient reactant specie. From this type of 1-D formulation, a relevant set of scaling parameters arises, facilitating the investigation of the large parametric space of the system. Based on the specific formulation employed by Lee and Maruta [31], the governing equations for gas species, gas energy, and wall energy can be written in a dimensionless form as follows:

$$U_b \frac{dY_f}{d\xi} = \frac{1}{Le}\frac{d^2Y_f}{d\xi^2} - \exp\left[\frac{\beta(\theta_f-1)}{2}\right]\delta(\xi-\xi_f), \tag{1}$$

$$U_b \frac{d\theta}{d\xi} = \frac{d^2\theta}{d\xi^2} - N_i(\theta-\theta_w) + \exp\left[\frac{\beta(\theta_f-1)}{2}\right]\delta(\xi-\xi_f), \tag{2}$$

$$U_p {R_\alpha}^{-1} \frac{d\theta_w}{d\xi} = \frac{d^2\theta_w}{d\xi^2} + R_{cr}N_i(\theta-\theta_w) - R_{cr}N_o\theta_w, \tag{3}$$

where the w subscript is used to denote wall properties. Flames are assumed to travel at a constant velocity, such that time dependent terms are expressed in terms of $U_p = S_p/S_{ad}$, which is the flame propagation speed normalized by the laminar burning velocity. The normalized burning velocity, U_b, corresponds to the sum of U_{in} and U_p. The axial coordinate, $\xi = x/\delta_f$, is normalized by the flame thickness, $\delta_f = \alpha/S_{ad}$, obtained from the ratio of gas thermal diffusivity over laminar burning velocity. In equation 1, Y_f corresponds to the normalized fuel mass fraction, while θ is a dimensionless fluid temperature obtained with the following scaling:

$$\theta = \frac{T-T_{in}}{T_{ad}-T_{in}}. \tag{4}$$

where T_{ad} is the adiabatic flame temperature, and T_{in} is the fluid inlet temperature, set to be equal to the temperature of the surroundings, T_∞, at which external heat loss occurs. In equation 1, unity Lewis number, $Le = 1$, is assumed. The chemical source term includes the Zeldovich number, $\beta = (E_a/R_u)(T_{ad}-T_{in})/T_{ad}^2$, with activation energy E_a and universal gas constant R_u. Dirac delta functions, δ, are used to represent point sources at the flame location, ξ_f, as the reaction zone is assumed to be infinitesimally thin.

The effect of thermal diffusivities of fluid and wall can be grouped into the ratio $R_\alpha = \alpha_w/\alpha$, while $R_{cr} = [kD^2]/[k_w({D_o}^2 - D^2)]$ is the thermal conduction ratio that takes into account the conductivities, k and k_w, and cross-sectional areas of fluid and wall. These two parameters, R_α and R_{cr}, are not directly related to

heat loss in the problem, and are kept constant throughout the study by keeping the fluid inlet properties and wall properties unchanged, and by keeping the ratio of outer diameter, D_o, to inner diameter, D, constant.

The only terms that are varied in this study are those related to convective heat transfer at the inner and outer wall surfaces, defined as

$$N_\mathrm{i} = \frac{4\,\mathrm{Nu_i}}{\mathrm{Pe}^2}; \qquad N_\mathrm{o} = \frac{4\,\mathrm{Nu_o}}{\mathrm{Pe}^2} \tag{5}$$

where Peclet number, $\mathrm{Pe} = D/\delta_\mathrm{f}$, is defined as the ratio of inner tube diameter to flame thickness. Nusselt number at the inner wall surface is defined as $\mathrm{Nu_i} = h_\mathrm{i} D/k$, where h_i is the convective heat transfer coefficient in $\mathrm{W/m^2/K}$. For the outer wall surface, $\mathrm{Nu_o} = h_\mathrm{o} D_\mathrm{o}/k$, where h_o is the external heat transfer coefficient that will be varied in this study.

It can be shown that N_i and N_o are effectively dimensionless expressions for volumetric heat transfer coefficients, whose units would be in $\mathrm{W/m^3/K}$. This volumetric expression allows the consideration of the change in external heat loss coefficient, h_o, as well as the change in surface-to-volume ratio associated with a change in tube diameter.

For the variation of heat loss over a range of tube diameters performed in this study, the focus is directed towards the variation of N_o, that will vary due to a change in both $\mathrm{Nu_o}$ and Pe. As diameter is varied, N_i also changes due to a change in Pe, while $\mathrm{Nu_i}$ is assumed to stay constant, as would be the case for thermally fully-developed laminar flow. This constant $\mathrm{Nu_i}$ assumption, present in the 1-D model, is expected to be most accurate in regions upstream and downstream of the flame zone, but does not allow for variations in $\mathrm{Nu_i}$ that can occur inside the thermally-developing flame zone [45, 46].

The asymptotic 1-D formulation leads to an eigenvalue problem which can be solved analytically. More details of this analytical solution can be found in [31]. This formulation, in which constant properties and simplified chemistry are used, is not as accurate as a 1-D numerical formulation, such as the one used in our previous study on the topic [32]. In the present study, the 1-D asymptotic model is utilized, not for quantitative predictions of flame properties, but for qualitative predictions of the observed trends, while providing a set of non-dimensional groupings by which the dominant physics of the system can be scaled.

2.2. Two-dimensional model

As a more detailed representation of the system, a 2-D elliptic model with conjugate heat transfer is used that is based on the Navier-Stokes equations for low-Mach-number reacting flows [32]. The multi-dimensional governing equations for mass and momentum are modeled as

$$\frac{\partial \rho}{\partial t} + \nabla \cdot (\rho \vec{u}) = 0, \tag{6}$$

and

$$\frac{\partial \rho \vec{u}}{\partial t} + \nabla \cdot (\rho \vec{u} \otimes \vec{u}) + \nabla \cdot \bar{\tau} = \rho \vec{g} - \nabla p, \tag{7}$$

respectively, where $\vec{u}$ is the velocity vector, ρ is the fluid density, and p is the static pressure. The viscous stress tensor, $\bar{\tau}$, is defined as $\bar{\tau} = -\mu[\nabla \vec{u} + \nabla \vec{u}^\mathrm{T} - \frac{2}{3}(\nabla \cdot \vec{u})\mathrm{I}]$, where μ is the fluid viscosity. Gravitational acceleration, g, is set to zero in this study.

Conjugate heat transfer is taken into account by coupling the gas energy equation to the solid energy equation at the fluid-wall interface. Conservation of energy is modeled as

$$\frac{\partial \rho h}{\partial t} + \nabla \cdot (\rho \vec{u} \cdot h) - \nabla \cdot (\rho \alpha \nabla h) = \frac{\partial p}{\partial t} + \vec{u} \cdot \nabla p + S_\mathrm{h}, \tag{8}$$

and

$$\frac{\partial(\rho_{\mathrm{w}} c_{\mathrm{w}} T_{\mathrm{w}})}{\partial t} - \nabla \cdot (k_{\mathrm{w}} \nabla T_{\mathrm{w}}) = 0, \tag{9}$$

for the gas and the solid, respectively. Equation 8 is expressed in terms of specific sensible enthalpy, h. The fluid thermal diffusivity is expressed as $\alpha = k/\rho c_p$. Heat production from chemical reactions is included in a heat source term, S_{h}, defined as

$$S_{\mathrm{h}} = -\sum_{i=1}^{N} h_{\mathrm{t},i} \dot{\omega}_i \tag{10}$$

where $h_{\mathrm{t},i}$ is the specific total enthalpy of species i, and $\dot{\omega}_i$ is the net production rate of that species. In Equation 9, wall properties, such as the solid thermal conductivity, k_{w}, and the solid heat capacity, c_{w}, are expressed with the subscript w. Wall properties ρ_{w}, c_{w}, and k_{w} are assumed to be constant. Fluid transport properties, such as thermal conductivity, k, and viscosity, μ, are mixture-averaged values that depend on the local mixture composition and temperature. Fluid density, ρ, varies based on the ideal gas law for the local mixture composition, temperature, and pressure. Fluid-wall coupling is captured by matching the heat flux and the temperature of adjacent solid and fluid phases at the fluid-wall interface. The external wall surface is subjected to a convective heat loss boundary condition, as shown in Fig. 1.

The 2-D model considers multiple species. Conservation of the local mass fraction, y_i, of each chemical species i is modeled as

$$\frac{\partial \rho y_i}{\partial t} + \nabla \cdot (\rho \vec{u} \cdot y_i) - \nabla \cdot (\rho \alpha \nabla y_i) = \dot{\omega}_i, \tag{11}$$

Because this study focuses of heat transfer interactions inside the system, and not on the additional effects associated with species differential diffusion, a unity Lewis number (Le=1) assumption is used, where species mass diffusivity is made equal to the fluid heat diffusivity. The reaction mechanism is chosen to be a reduced 2-step mechanism for methane by Westbrook and Dryer [47] that includes 5 species. Surface reactions are not included in the present formulation because an inert non-catalytic wall material is considered [25], and because the relative influence of radical quenching becomes negligible at the high wall temperatures that are modeled [19].

The fluid-wall system is assumed to be axisymmetric, allowing the 2-D modeling of only a sector (wedge) of the circular tube cross-section. At certain conditions, flames in small tubes or channels can present asymmetric flame structures [23, 48–53]. Asymmetries have been reported in situations involving non-unity Lewis number mixtures [27, 48–52], flame instabilities [52, 54, 55], the influence of gravity [30, 54], and relatively low wall temperatures [23, 53]. In this study, unity Le is assumed, only stable flames are considered, gravity is neglected, and high wall temperatures, associated with heat-recirculation, are obtained; therefore, the flames are expected to be axisymmetric. To verify this assumption, some 3-D simulations are performed to cover the range of tested conditions, as described in Appendix A. All the obtained 3-D results are observed to be stable and axisymmetric. More information about the multi-dimensional model implementation and solving procedure can be found in [32].

2.3. Investigated conditions

The conditions used in this study are similar to those used in our previous study on the topic [32], in which the influence of external heat loss was not considered. Fixed values of species mass fraction, velocity and temperature are specified at the tube inlet, and atmospheric pressure is specified at the tube outlet

for the 2-D model. Only stoichiometric methane-air mixtures are studied, where the inlet mass fractions of methane (CH_4), oxygen (O_2), and nitrogen (N_2), are 0.055, 0.220, 0.725, respectively.

The inlet temperature, T_{in}, and external surrounding temperature, T_∞, are set to 900 K. This high ambient temperature, while below the point of auto-ignition of the mixture, is chosen in order to reflect the conditions that would prevail in the case of external heat transfer to a high-temperature heat load. In order to reach this elevated inlet temperature of 900 K, an external heat exchanger can be used to preheat the incoming reactant stream, using heat from the combustion-product stream [56, 57].

Inner tube diameter, D, is varied between 0.1 and 5.0 mm and wall thickness is kept equal to half of the inner tube radius, as shown in Fig. 1. Wall properties are the same as quartz, except that density and heat capacity are both reduced by a factor of 10 ($k_{\text{w}} = 1.1$ W/m/K, $\rho_{\text{w}} = 265$ kg/m^3, $c_{\text{w}} = 75$ J/kg/K). This leads to an increase in propagation velocity of thermally-coupled flames, facilitating the computational assessment of propagation speed, which would otherwise require longer run times. By considering the heat flux associated with the propagation of a thermal wave inside the wall to be equal to the heat absorbed at the inner tube surface through convective heat transfer along the thermal wave thickness, $\delta_{\text{w}} = \alpha_{\text{w}}/S_{\text{p}}$, the wall thermal wave speed can be approximated as follows [30]:

$$\frac{\pi(D_{\text{o}}^2 - D^2)}{4}\rho_{\text{w}} S_{\text{p}} c_{\text{w}} \Delta T = \pi D \frac{\alpha_{\text{w}}}{S_{\text{p}}} h_{\text{i}} \Delta T \tag{12}$$

$$S_{\text{p}} = \frac{2}{\rho_{\text{w}} c_{\text{w}}} \sqrt{\frac{k_{\text{w}} k \,\text{Nu}_{\text{i}}}{(D_{\text{o}}^2 - D^2)}} \tag{13}$$

It can be seen that the reduction in heat capacity of the wall, $\rho_{\text{w}} c_{\text{w}}$, leads to an increase in propagation velocity, S_{p}. This resulting increase in S_{p} is expected to have a limited impact on flame spatial profiles, since the timescale of the thermal wave at the simulated conditions,, $t_{\text{w}} = \alpha_{\text{w}}/{S_{\text{p}}}^2 \sim \mathcal{O}(10^{-4})/\mathcal{O}(10^{-2})^2 \sim \mathcal{O}(10^0)$ s, remains much greater than the flame timescale, $t_{\text{f}} = \alpha/{S_{\text{ad}}}^2 \sim \mathcal{O}(10^{-4})/\mathcal{O}(10^0)^2 \sim \mathcal{O}(10^{-4})$ s, and the conduction timescale, $t_{\text{c}} = D^2/\alpha \sim \mathcal{O}(10^{-3})^2/\mathcal{O}(10^{-4}) \sim \mathcal{O}(10^{-2})$ s.

Additionally, the length-scale of the thermal wave, $\delta_{\text{w}} = \alpha_{\text{w}}/S_{\text{p}}$, using Equation 13, can be written as follows:

$$\delta_{\text{w}} = \frac{1}{2}\sqrt{\frac{k_{\text{w}}(D_{\text{o}}^2 - D^2)}{k \,\text{Nu}_{\text{i}}}} \tag{14}$$

Since δ_{w} is predicted to be independent of a change in ρ_{w} and c_{w}, the change in wall heat capacity is expected to have a negligible impact on wall spatial profiles. It should additionally be noted that stationary flame predictions, at which slow flames transition from upstream to downstream propagation, are not affected by this change in wall heat capacity, because only the wall thermal conductivity, k_{w}, influences the steady-state solution, as seen in Eq. 9.

The average inflow velocity, S_{in}, is set to 10 m/s for all cases, which is 3.15 times greater that the adiabatic laminar flame speed predicted at inlet conditions, $S_{\text{ad}} = 3.17$ m/s. This specific inflow velocity is chosen in order to ensure that all the simulated flames are stable, strongly-burning, and within the slowly-propagating flame regime [32]. These strongly-burning heat-recirculating stable flames are of interest for power production at high energy densities. While temporal instabilities, such as periodic oscillations [36], can be resolved with the 2-D transient model used in this study, only stable flames are obtained over the range of tested conditions.

In the 1-D asymptotic model, gas properties are assumed to be constant, and based on the stoichio-

metric methane-air mixture properties at T_{in}. The chemical heat release per unit mass of fuel is set to $4.335 \cdot 10^4$ kJ/kg, and the activation energy of chemical reaction is set to $E_{\text{a}} = 200.1 \cdot 10^2$ kJ/mol/K. This choice of model parameters leads to adiabatic flame properties of $S_{\text{ad}} = 3.17$ m/s, $T_{\text{ad}} = 2728$ K, $\delta_{\text{f}} = 44.8$ μm, that are equal to the adiabatic flame properties predicted with the 2-D model with 2-step chemistry. It should be noted that $\delta_{\text{f}} = \alpha / S_{\text{ad}}$ is obtained for the 2-D model based on the value of α calculated at inlet conditions.

Characteristic flame thickness can alternately be calculated based on temperature gradient and temperature rise across an adiabatic laminar flame, as performed in [32]. This alternate thermal flame thickness value, $\delta_T = 195$ μm, differs from δ_{f} for the 2-D model. For the 1-D asymptotic model, δ_T and δ_{f} predictions are equal, due to assumptions in the model formulation. In this study, the value of $\delta_{\text{f}} = \alpha / S_{\text{ad}}$ is chosen as the characteristic flame thickness, in order for 1-D and 2-D modeling results to be compared at equivalent conditions with respect to the scaling parameters involved in the 1-D asymptotic model formulation.

In addition to ensuring equivalent adiabatic flame properties between the models, quenching diameter predictions are also made equal between models [32]. The evaluation of quenching diameter provides a relevant assessment of flame-wall thermal interactions, as it depends on the rate balance between heat release and interfacial heat transfer across the flame [13]. A value of $\text{Nu}_{\text{i}} = 5.73$ is chosen such that the 1-D model predicts quenching to occur at the same $\text{Pe}_{\text{q}} = 27.1$ value as the 2-D model. This ensures that the 1-D and 2-D flames are influenced by interfacial heat transfer in a similar manner. The matching of Pe_{q} between models is additionally important because Pe_{q} is a critical parameter bounding the occurrence of different burning regimes in the system [28, 32], where conventional rapidly-propagating uncoupled flames can only exist when $\text{Pe} \geq \text{Pe}_{\text{q}}$.

2.4. Characteristic flame structure

Figure 2 shows typical radially-averaged solution profiles obtained with the two different models, for $D = 0.1$ mm, and $h_{\text{o}} = 50$ W/m^2/K. Results are presented in terms of dimensionless gas temperature, θ, wall temperature, θ_{w}, deficient species mass fraction, $Y_{\text{f}} = y_{\text{CH}_4} / y_{\text{CH}_4\,\text{in}}$, and dimensionless total enthalpy, H. Total enthalpy, h_{t}, which is the sum of sensible enthalpy, h, and chemical enthalpy, h^{o}, is made dimensionless using the following expression:

$$H = 1 + \frac{h_{\text{t}} - h_{\text{t,in}}}{h^{\text{o}}_{\text{in}} - h^{\text{o}}_{\text{out,ad}}} \tag{15}$$

where the difference between local total enthalpy and inlet total enthalpy is divided by the specific energy release of an adiabatic laminar flame. The value of H would remain constant at unity across an adiabatic $\text{Le} = 1$ flame. H is greater than 1 when excess enthalpy occurs in the system, and heat loss to the wall can reduce this value below unity. As the two-dimensional model produces radially-varying profiles, it is the bulk radially-averaged values, denoted with an overline, that are plotted in Fig. 2 (a), based on the weighted averages described in [32].

Axial flame solutions of temperature, deficient species, and enthalpy, obtained with the 2-D and 1-D models, can be seen in Fig. 2. Upstream of the flame, both models predict a preheat zone where the wall temperature is greater than the fluid temperature, and where excess enthalpy occurs, with $H > 1$. At the flame zone, chemical heat release from fuel consumption allows the fluid temperature to become greater than the wall temperature, reversing the direction of interfacial heat transfer. The post-flame region is characterized by a decrease in temperature and enthalpy, as the fluid loses heat to the wall that is losing heat to the surroundings. The 1-D asymptotic model significantly overestimates the peak flame temperature. This can be related to the infinitesimally thin flame assumption that prevents heat loss to be accurately

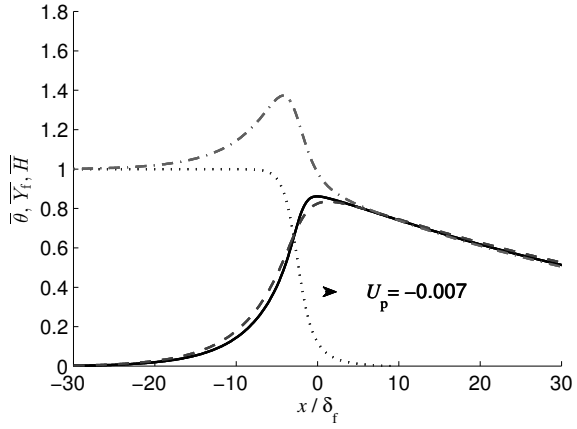

(a) 2-D

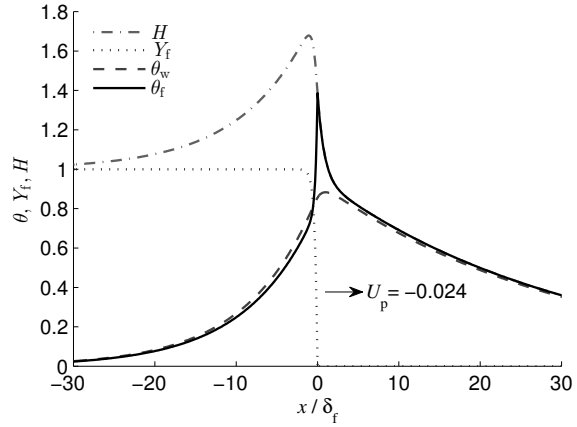

(b) 1-D

Figure 2: Axial flame solutions obtained with the 2-D (a) and 1-D (b) models. Profiles of radially-averaged dimensionless fluid temperature, θ, wall temperature, θ_w, fuel mass fraction, Y_f, and total enthalpy H are shown for both models. Both flames travel at a specific dimensionless propagation velocity, U_p. Simulations are performed for a tube of 0.1 mm inner diameter, with an external heat loss coefficient of 50 W/m^2/K, and an inflow velocity of 10 m/s.

resolved within the flame zone [46, 58]. The fuel consumption zone is, accordingly, thinner for the 1-D model predictions. Both models predict a steady flame propagation in the downstream direction, but the predicted values of U_p differ.

The axial flame profiles show that, despite shortcomings in terms of simplifying assumptions, the 1-D model is able to capture important physics pertaining to excess enthalpy and heat loss in the system. This type of formulation has been extensively used to map the system behavior over a wide range of conditions [18, 29, 31, 39]. In this study, the qualitative trends predicted by the 1-D asymptotic model are used as a hypothesis for the behavior of the system over the range of tested conditions. The qualitative discrepancies between predicted trends are used in the assessment of the influence of 2-D effects on the behavior of the system.

3. Results and discussion

3.1. Effect of heat loss on flame propagation and quenching

Predictions of propagation velocity, S_p, as a function of external heat loss coefficient, h_o, are shown in Fig. 3 (a) for six different tube diameters. Two-dimensional results are shown as thick lines, while 1-D results are shown as dashed lines. Heat loss is seen to reduce the propagation velocity of flames. This decrease steepens when approaching the limit of propagation. The direction of flame propagation can change with an increase in heat loss coefficient, from upstream propagation, to a stationary solution, to a downstream propagation. The stationary flame solutions correspond to the crossing points of solution curves with the thin dotted line $S_\mathrm{p} = 0$.

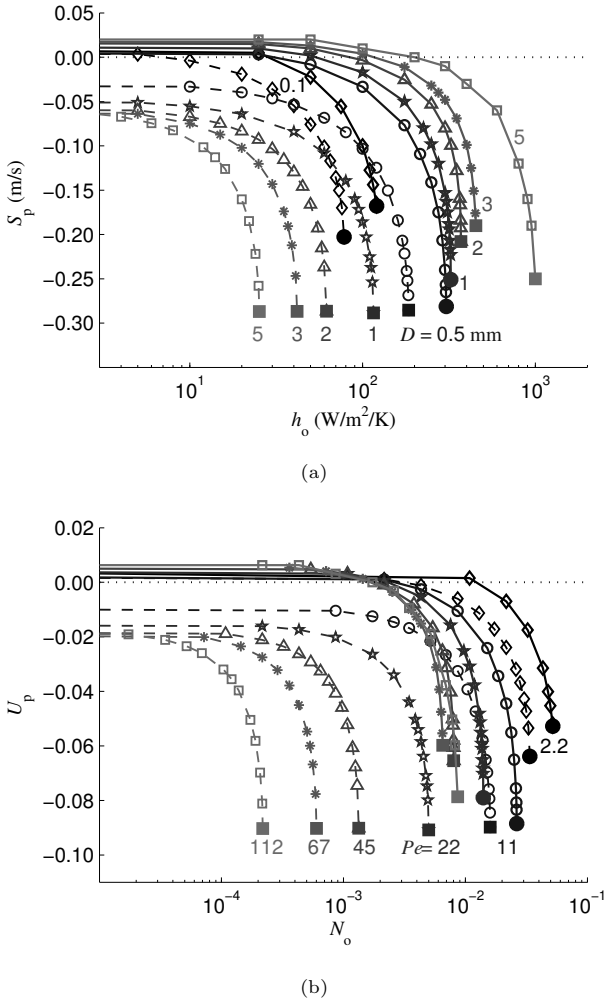

Figure 3: Dependency of propagation speed, S_p, on heat loss coefficient, in terms of dimensional (a), and dimensionless (b) parameters, for the 1-D (dashed lines), and 2-D (thick line) model predictions, for a range of inner tube diameters. Extinction limits are shown as filled circles, while blowout limits are shown as filled squares.

Two types of heat loss limits are observed in this study: extinction and blowout. This is consistent with previous findings on heat-recirculating burner systems [35, 36]. Extinction occurs when the rate of heat release by combustion becomes too small to overcome heat loss due to a global reduction in flame temperatures [36]. Blowout refers to the case where residence time in the preheat zone becomes too small for the flame to stay

coupled to the wall temperature profile. In the figures, extinction limits are denoted with filled circles, while blowout limits are shown with filled squares.

The nature of heat loss limits is verified through a slight variation of the inlet velocity at heat loss limit conditions. Extinction limits occur at the low end of the range of permissible inflow rates, such that flames can only be obtained at higher inflow velocities, $U_{\mathrm{in}} > 10$ m/s. Inversely, blowout limits occur at the high end of the permissible inflow range, such that thermally-coupled flames can only be obtained for $U_{\mathrm{in}} < 10$ m/s.

In Fig. 3 (a), it can be seen that the two models predict extinction limits at small diameters and blowout limits at larger diameters. However, the type of predicted limits differs between models for the $D = 0.5$ and $D = 1.0$ mm cases, where the 2-D model predicts extinction limits instead of blowout limits. Both models predict the same qualitative decrease in S_{p} due to an increase in h_{o}. However, while the trends in predicted h_{o} value at the limit are similar for both models at small diameter values, of $D = 0.1$ and $D = 0.5$ mm, the 1-D model is unable to predict the increase of stability observed at larger diameters. This indicates that 2-D effects, which become increasingly important at larger tube diameters [32], allow flames to sustain more heat loss than predicted by the classical 1-D depiction of the problem.

The variation of normalized propagation speed, U_{p}, as a function of dimensionless heat loss, N_{o}, is shown in Fig. 3 (b). Again, propagation speed is seen to decrease with an increase in heat loss coefficient. At small Pe, both models predict a decrease in N_{o} limits with increasing Pe. However, at larger diameters, the blowout limits predicted with the 2-D model converge to an approximately constant value of $N_{\mathrm{o}} \approx 10^{-2}$. This suggests that there exists, for this particular set of conditions, an approximately constant blowout limit that is independent of diameter. This can be linked to 2-D effects that cannot be captured with the 1-D formulation, which instead predicts a monotonic decrease in maximum permissible volumetric heat loss coefficient, N_{o}, at the meso-scale.

The dependence of heat loss limits on the change in tube diameter is plotted in Fig. 4. Heat loss limits of downstream propagating flames are denoted with black symbols, while stationary flame conditions are shown in grey color. The quenching diameter of the mixture calculated at inlet conditions, $D_{\mathrm{q}} = 1.216$ mm, normalized as Pe_{q}, is shown as thin dotted lines to denote the characteristic dimension differentiating the micro- and meso-scales of the system [16].

Stationary flame conditions are relevant to steady-state burner operation with continuous inflow, where downstream propagating flames ultimately leave the burner structure. The quenching limits of downstream propagating flames, on the other hand, are relevant to the operation of heat-recirculating burners with periodic flow reversal [59, 60]. While the 2-D model predicts upstream propagating flames at adiabatic conditions, for all tested tube diameters at the constant inflow velocity of 10 m/s, the 1-D model only predicts upstream propagating flames over a range of diameters, leading to a narrower range of stationary solution predictions.

The value of convective heat loss parameter at the stationary condition and at the propagation limit is plotted in Fig. 4 (a) as a function of tube diameter. The 1-D model predicts the existence of an optimal diameter value at which stability is maximized, which was previously observed for a comparable heat-recirculating burner configuration, based on 1-D model predictions [40]. The two-dimensional model, however, predicts a monotonic increase of the quenching limit with diameter. For diameters greater than the 1-D optimum value, the prediction curves diverge from one another. The difference is most pronounced at the meso-scale, but also exists at the upper range of the micro-scale. This shows that 2-D effects can have a significant influence on stability, even at diameters smaller than the quenching distance. Similar trends can be observed for the stationary flame condition results, where the 2-D model predicts a continuous increase in permissible h_{o} when diameter is increased. Contrastingly, the 1-D model predicts a peak in permissible h_{o}, and only

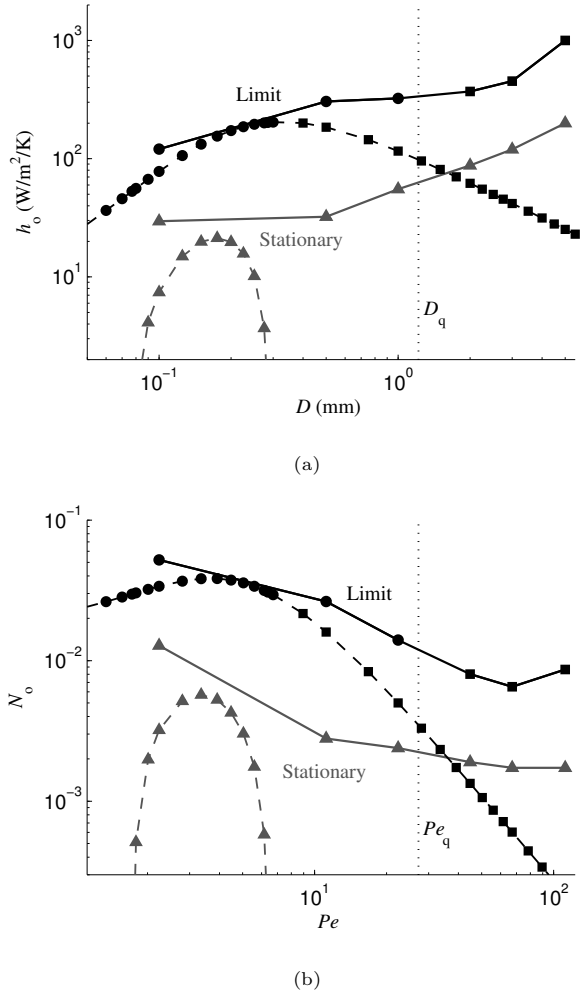

Figure 4: Heat loss parameters, h_o and N_o, at heat loss limits, and at the stationary flame conditions, as a function of inner tube diameter, in dimensional (a) and dimensionless form (b), for the 1-D (dashed-line), and 2-D (thick-line) model predictions. Extinction limits are shown as circles, while blowout limits are shown as squares. 2-D stationary flame data is interpolated between upstream and downstream propagation velocity results.

predicts stationary solutions to occur over a restricted range of small tube diameters.

The limits can also be expressed in terms of N_o as a function of Pe, as shown in Fig. 4 (b). Two-dimensional results show that both the stationary and the downstream propagation N_o limits decrease with increasing Pe, until an approximately constant value of N_o is reached at larger Pe. Blowout limits, indicated as squares, all occur in the meso-scale range, at similar values of N_o. This suggests that an approximately constant N_o value can be used to predict the blowout limit at the meso-scale, at least for a particular set of conditions. Similarly, an approximately constant N_o value can be found for the stationary flame condition at the meso-scale. The 1-D model does not capture these trends, as it predicts an optimum Pe at small diameters, and a continuous decrease in quenching limits at larger diameters. The 1-D model does not predict any stationary, or upstream propagating, flames at the upper range of micro-scale, nor at the meso-scale. These significant discrepancies between trends in model predictions indicate that 2-D effects play a significant role at the meso-scale, but also at the upper-range of the micro-scale.

When considering the type of quenching limits of flames, it can be seen that tubes at the micro-scale,

with $d < D_q$, are subjected to an extinction limit, while tubes at the meso-scale, with $d > D_q$, are subjected to a blowout limit. This is consistent with the concept of quenching distance, where flames are expected to exhibit global extinction in channels smaller than D_q. However, the flames at the micro-scale can also reach a blowout limit at larger inflow velocities. For a specific inflow velocity at a set of conditions, a specific diameter value can be found that separates extinction from blowout limits. This diameter value is velocity dependent, and cannot be assumed to be equal to D_q, but is seen to be close to it in this moderately-high inlet velocity case where $S_{in} = 3.15\, S_{ad}$.

3.2. Effect of heat loss on flame properties

In this section, flame solutions are examined to determine the changes in flame properties that cause the observed influence of heat loss on flame propagation and quenching. Figure 5 shows contour plots of dimensionless temperatures, θ and θ_w, and total enthalpy, H, of flames obtained at three different diameters, $D = 0.1$, $D = 0.5$, and $D = 2.0$ mm. For each diameter, two cases are shown, the adiabatic flame case and the extinction/blowout limit case.

As tube diameter is enlarged, flames are seen to become increasingly elongated as the flame front becomes increasingly parallel to the wall surface. In addition, zones of excess enthalpy become more concentrated at the fluid/wall interface. This was previously observed at adiabatic conditions [32], where the flame shapes are reminiscent of those stabilized on Bunsen burners, with flame-normal burning velocities close to the laminar burning velocity [32].

When flames are subjected to heat loss, it can be seen in Fig. 5 that the axial thickness of the wall thermal wave increases. This is mainly due to the decrease in flame propagation speed associated with an increase in heat loss. As S_p decreases, or increases in the negative direction, the rate of upstream axial transport of heat inside the solid structure, in the reference frame of the moving flame, is effectively increased. This lengthens the wall preheating zone, leading to a thickening of the excess-enthalpy zone, $H > 1$, shown in shades of gray. The thickness of the wall thermal wave is seen to also increase with tube diameter, for both adiabatic and heat loss cases. This is consistent with an increase in wall thickness, $t_w = D_o - D = D/4$, that leads to an increase in area available for axial conduction, $\pi(D_o^2 - D^2)/4$, as seen in Eq. 14.

Temperature is seen to decrease with heat loss, with maximum temperatures occurring at the centerline. The effect of heat loss on the flame becomes more localized at the flame-wall interface when tube diameter is made larger. The $D = 0.1$ and $D = 0.5$ mm cases are subjected to an extinction limit, and the extent of the temperature decrease impacts most of the flame surface area, with radially-distributed zones of lowered temperatures. For the $D = 2.0$ mm case, which is subjected to a blowout limit, only a ring of fluid close to the wall is subjected to a significant decrease in flame temperature due to heat loss. Simultaneously, excess enthalpy is concentrated in this same ring of fluid, allowing for the onset of combustion to take place close to the wall. From this ignited zone, heat travels at a limited rate towards the center-line, leading to the observed elongated flame shape [32]. Accordingly, the phenomena responsible for inducing heat loss limits to excess-enthalpy flames at larger diameters are expected to occur within this ring of fluid close to the wall. In 1-D model formulations, it is assumed that the bulk of the flow, and not a localized portion of it, is affected by wall heating and heat loss. This implies that the effect of heat loss at larger diameters can only be evaluated accurately using a 2-D formulation. These localized effects at large diameters lead to an increase in flame stability, as seen in Fig. 4 (a).

For the $D = 2.0$ mm case, the wall temperature is seen to vary significantly in the radial direction. Maximum wall temperatures occur at the fluid/wall interface, away from the external surface where heat loss

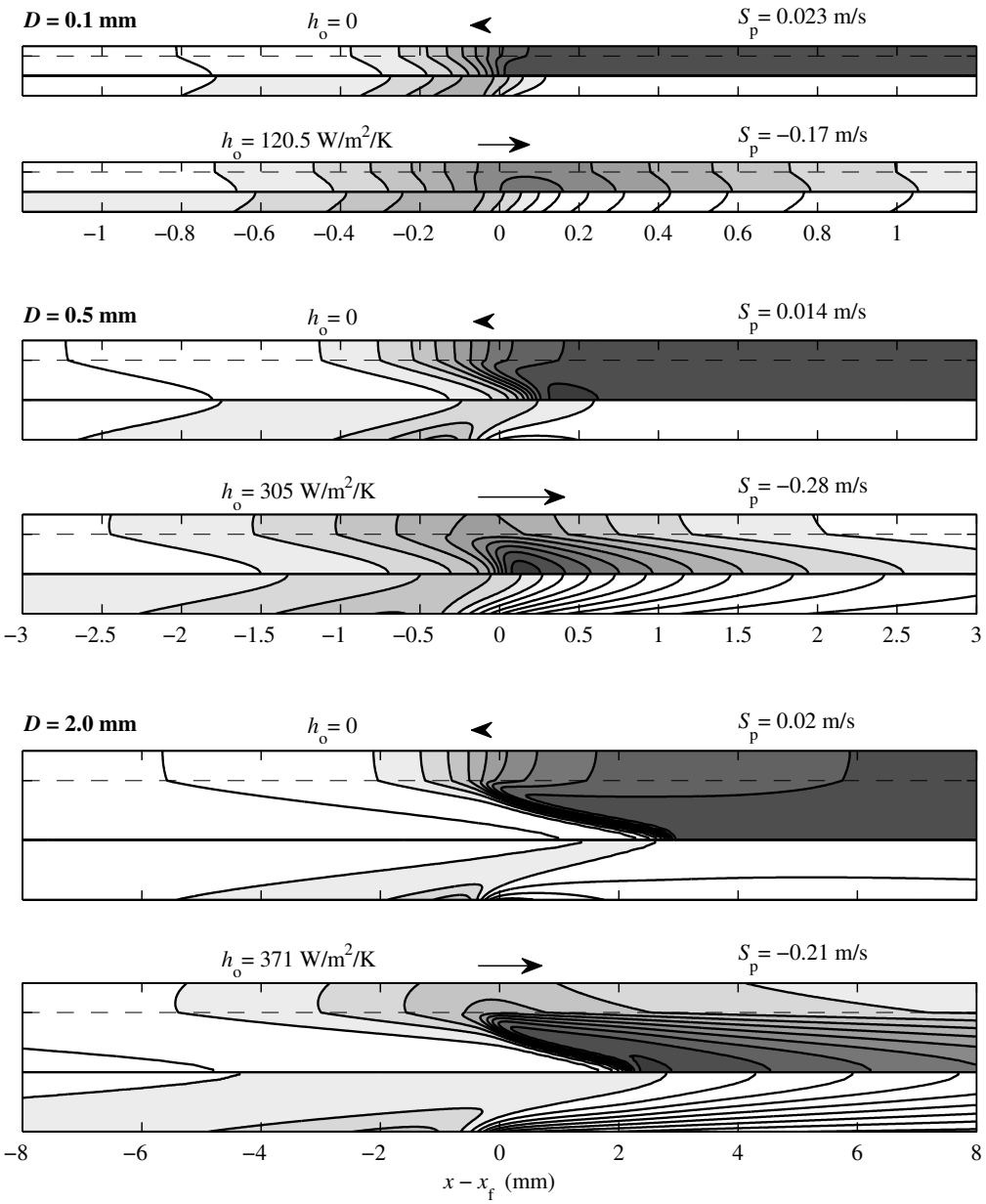

Figure 5: Contour plots of normalized temperature, θ, of both fluid and wall (upper half), and total enthalpy, H, of the fluid only (lower half), for three different inner tube diameters, D = 0.1, 0.5, and 2.0 mm. For each of the three diameters, the adiabatic case is shown above the highest-permissible-heat-loss case. Iso-contours are shown at intervals of 0.1 of the normalized parameters. Gray color scaling is used for values above 0.2 for temperature, and for values above 1.0 for enthalpy.

takes place. Radial thermal gradients indicate that the wall provides a significant thermal resistance between the inner and outer wall surfaces, which cannot be captured with 1-D models where the wall is assumed to be thin. This insulating effect, associated with increased wall thickness, partly contributes to the greater

stability observed at larger diameters.

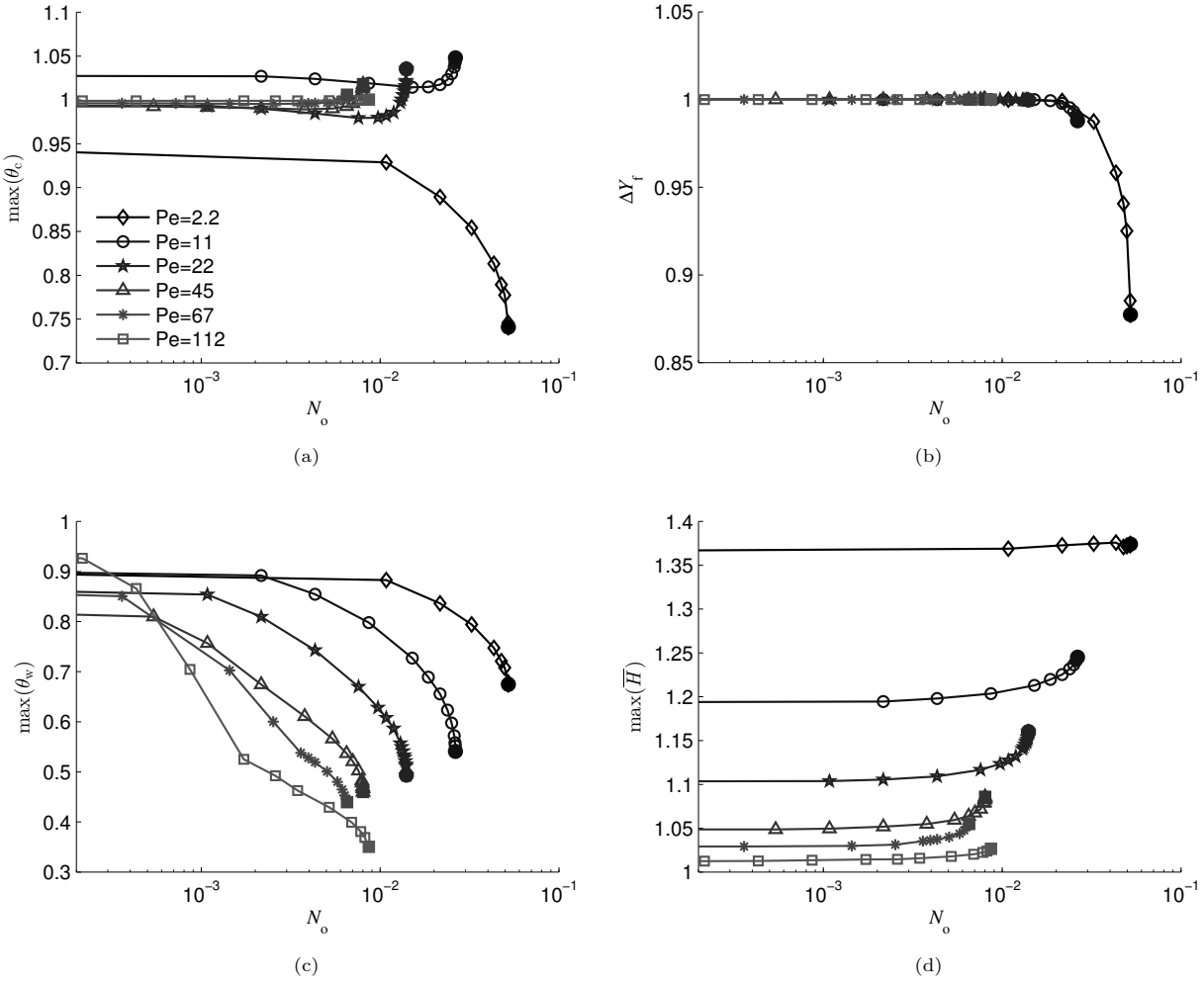

Figure 6: Influence of non-dimensional heat loss parameter on normalized maximum center-line temperature, $\max(\theta_c)$, in (a), on total fuel consumption, $\max(\Delta Y_f)$, in (b), on maximum wall interface temperature, $\max(\theta_r)$, in (c), and on maximum total enthalpy, $\max(\overline{H})$, in (d). Results are shown for different values of Pe, corresponding to the different tube diameters tested with the 2-D model. Extinction limits are shown with filled circles, while blow-off limits are shown with filled squares.

Dimensionless flame properties are plotted in Fig. 6 as a function of dimensionless heat loss parameter for different values of Pe. Maximum centerline temperature is plotted in Fig. 6 (a) in order to assess the influence of heat loss on flame temperature. For the smallest diameter (and Pe) case, maximum center-line temperature is seen to decrease significantly with an increase in heat loss. This is attributed to the small diffusion distance between wall and center-line at small diameters, that leads to greater radial uniformity of the profiles and a significant temperature reduction at the tube center-line. As diameter is slightly increased, for Pe = 11 and 22, this uniformity diminishes, and center-line temperature behavior changes. Center-line temperature decreases slightly with an increase in heat loss until it approaches the extinction limit, where an increase in center-line temperatures is observed. This increase in maximum flame temperature at the extinction limit is associated with the sharp decrease in S_b at the limit, that leads to longer preheating lengths and more preheat reaching the center-line. However, as seen in Fig. 5 for the $D = 0.5$ mm case, center-line temperature is not representative of the average flame temperature at the extinction limit, since

significant radial non-uniformities in temperature profiles are observed in this upper range of the micro-scale. Superadiabatic center-line temperatures are also observed for these cases at the upper-range of the micro-scale, indicating that wall preheating associated with heat recirculation influences the totality of the flow, from wall to center-line. In contrast, at larger diameters, subjected to a blowout limit, the influence of the wall, through heat recirculation or heat loss, has a much reduced impact on the center-line temperature. For the meso-scale cases with $\mathrm{Pe} > \mathrm{Pe_q} = 27.1$, maximum flame temperatures are very close to the adiabatic flame temperature, and stay more or less constant with an increase in heat loss.

The significant decrease in flame temperatures observed for the smallest diameter case leads to a significant amount of un-reacted fuel, $\Delta Y_\mathrm{f} < 1$, as seen in Fig. 6 (b). Therefore, for the smallest diameter case, the extinction limit can be linked to a reduction in fuel consumption due to reduced temperatures and reaction rates. As diameter is increased, extinction limits are not necessarily linked to a drop in fuel conversion, as seen for the $D = 1.0$ mm, $\mathrm{Pe} = 22$ case. In that case, some fuel is un-reacted in the vicinity of the wall as it leaves the flame front, but has sufficient time to diffuse and react further downstream in the high temperature region trailing the flame front. The length of this high-temperature region increases with diameter, due to a reduction in fluid cooling rates associated with an increase in tube diameter. At the blowout limits, fuel is seen to be fully consumed as ΔY_f stays unchanged.

Maximum wall interface temperatures, $\max(\theta_\mathrm{r})$, are plotted in Fig. 6 (c), in order to provide a measure of the temperature at which preheat occurs. Each tube diameter case quenches at a different interface temperature. Larger tube diameters allow for lower wall temperatures at the limit. For all diameter cases, maximum wall interface temperatures are seen to decrease with heat loss, which would be expected to lead to a drop in heat recirculation. However, heat recirculation is seen to stay more or less constant with an increase in heat loss, as shown in Fig. 6 (d) with maximum average total enthalpy, $\max(\overline{H})$. Excess enthalpy is even seen to increase close to the extinction/blowout limit, due to the sharp decrease in S_p. This indicates the flame is able to compensate for the reduction in preheat temperatures by a decrease in S_p that lengthens the preheat zone. Ultimately, the flame reaches a heat loss limit when wall temperature is too low to sufficiently preheat the mixture within the residence time associated with the preheat length.

This compensating effect between preheat length and preheat temperature leading to heat loss limits is influenced by the magnitude of heat recirculation occurring in the system. It can be seen in Fig. 6 (d) that the proportion of heat recirculated decreases with an increase in tube diameter, despite the fact that all cases have similar burning rates $S_\mathrm{b} \approx S_\mathrm{in}$. This is consistent with the previous observation that, as diameter is increased, the increase in flame burning rate depends decreasingly on wall preheating, and increasingly on flame area increase [32]. The lower amount of preheat required for large-diameter tubes, in addition to their longer preheat lengths associated with thicker walls, allows them to maintain lower wall temperatures at the blowout limit, as observed in Fig. 6 (c).

Heat loss limits in heat-recirculating burners have previously been linked to an approximately constant minimum flame temperature [33]. It is relevant to determine if a minimum flame temperature is observed in the current simulations. Radially-averaged temperature values cannot be considered as characteristic flame temperatures as soon as flame elongation is present, as it merges reacted and un-reacted zones together. Consequently, center-line and interface temperatures are considered as characteristic flame temperatures, that are not based on any radial averaging of the flow. At the quenching limits, both center-line and interface temperatures are seen to vary with tube diameter, as seen in Fig. 6 (a) and (c). The present results do not support the hypothesis of an approximately constant minimum flame temperature. It should be noted, however, that the two-steps reaction mechanism used here, while expected to capture the global characteristics

of the flame zone, does not capture the details of methane decomposition that can occur in the preheat zone, near the high-temperature fluid-wall interface [41]. This could influence the conditions associated with the onset of combustion at the wall. The significance of this additional effect is expected to be small at the short residence times associated with the high flow rates of strongly-burning excess-enthalpy flames.

3.3. Design implications

The conditions tested in this study, involving fixed inflow velocity, composition and geometry, allow for tubes of different diameters to be compared at the same volumetric heat input, in $\mathrm{W/m^3}$. Assuming that, in a practical system, an external heat load requires a fixed power input, and that a fixed burner volume is needed to satisfy space constraints, results at constant volumetric heat input can serve to determine the most advantageous tube diameter to be used in a tube bundle, consisting of a grouping of individual tubes [56], occupying the prescribed burner volume. The thermal resistance of the interface between outer tube surface and heat load can be translated into a corresponding heat loss coefficient at the outer tube surface.

When considering heat loss limits expressed in terms of dimensionless volumetric heat loss coefficient, smaller tubes, at the micro-scale, are seen to allow for greater values of N_o, which leads to higher volumetric power density for heat transfer. Nevertheless, larger tubes, at the meso-scale, can have higher performance than anticipated with 1-D modeling results. For these larger tubes, an approximately constant value of N_o is reached at blowout, which can simplify the design approach at the meso-scale.

Since stability, associated with a maximum permissible h_o, is observed to increase with tube diameter, it may be advantageous to go to larger tube diameters to prevent flame quenching caused by uneven heat loss distribution. The drop in fuel conversion observed at the extinction limit for the smallest diameters would lead to undesirable unburned hydrocarbon emissions. This reduces the range of permissible heat loss for these small-diameter cases. Other considerations should be taken into account in burner design, such as minimizing the pressure drop, which increases with a decrease in tube diameter, and restricting burner length. The required burner length depends on both the length of the flame, which should be contained within the burner structure, and the length over which the heat generated inside the fluid can be transferred to the wall. These two length scales increase when tube diameter is increased.

When considering power density, flame length, and heat transfer length, smaller diameters are favored. When considering flame stability, pressure drop, and fuel conversion, larger diameters are favored. This suggests that an optimal diameter value could be determined that would likely be close to the transition between the micro- and meso-scale, with the quenching diameter commonly used to define the transition between these two scales [16].

In order to determine an exact value, an optimization procedure should be performed based on predictive tools that can accurately capture the behavior of the system over a sufficient range of tube diameters. The computationally efficient 1-D model cannot be used over a significant range of tube diameters. It is unable to capture changes in flame surface area, that allow upstream and stationary flame solutions to exist at larger tube diameters, and that significantly modify the impact of heat loss on the system. This leads to significant inaccuracies in 1-D predictions of flame behavior and heat loss limits at larger tube diameters.

4. Conclusion

In this study, the slow propagation of flames inside heat-recirculating tubes is investigated using a detailed 2-D model with conjugate heat transfer, in order to accurately capture the influence of heat loss on flame behavior and propagation limits, for a range of tube diameters spanning the micro- and the meso-scale.

An increase in external heat loss leads to a decrease in propagation speed of the slowly-propagating flames, until a heat loss limit is reached. For smaller tube diameters, in the micro-scale range, flames are subjected to an extinction limit, while larger diameter tubes, in the meso-scale range, are subjected to a blowout limit. The values of external heat loss coefficient, h_o, at these extinction/blowout limits, increases with tube diameter, leading to greater stability of the system at larger diameters. Smaller tubes, on the other hand, allow for larger values of dimensionless volumetric heat loss coefficient, N_o, at the limit. When tube diameter is increased, the limit value of N_o decreases until an approximately constant value is reached at blowout, in the meso-scale range. This suggests that an approximately constant blowout limit, expressed as a N_o value, can be found at the meso-scale, at least for a particular set of conditions. Similarly, an approximately constant stationary flame condition, expressed as a N_o value, is also observed at the meso-scale.

These trends observed at larger diameters cannot be predicted with the 1-D asymptotic model used in this study as a hypothesis for the qualitative behavior of the system. These discrepancies in the predicted trends indicate that 2-D effects play a significant role at larger diameters, not only at the meso-scale, but also in the upper-range of the micro-scale, for both the stationary and downstream-propagating flame predictions. Two-dimensional effects, associated with changes in flame shape that enable an increase in flame burning area, are seen to significantly promote stability of the system.

Flame/wall solutions are further investigated in order to examine the influence of heat loss on flame characteristics. Flames at smaller diameters experience heat loss throughout the flame structure, which can lead to un-reacted fuel in the system. Flames at larger diameters are only influenced by wall heat loss in a localized region near the fluid/wall interface. For all tested tube diameters, the decrease in propagation speed associated with an increase in heat loss leads to a lengthening of the wall preheating zone, allowing the amount of heat-recirculation in the system to remain approximately unchanged, and to even increase close to the heat-loss limit. Maximum wall temperatures, on the other hand, are significantly reduced by heat loss, and larger tube diameters are seen to allow for lower wall temperatures at the heat loss limits.

These results have implications on the choice of tube diameter to be used in the design of a stable burner optimized for heat transfer to an external heat load, such as an external combustion engine.

Acknowledgments

We are grateful for the assistance of Gideon Balloch in the development of the 2-D numerical tool used here. Computations were made on the supercomputer Colosse from Université Laval, managed by Calcul Québec and Compute Canada. The operation of this supercomputer is funded by the Canada Foundation for Innovation (CFI), Ministère de l'Économie, de l'Innovation et des Exportations du Québec (MEIE), RMGA, and the Fonds de Recherche du Québec - Nature et Technologies (FRQ-NT). Funding from the Natural Sciences and Engineering Research Council of Canada (NSERC) is gratefully acknowledged.

Appendix A: Three-dimensional simulations and axisymmetric flame assumption

In order to verify the axisymmetric assumption used in this work, 3-D simulations of the fluid phase are performed. The numerical model used is the same as the one described in Section 2.2, with the difference that the wall energy equation, Eq. 9, is not solved. Instead, the wall temperature profile, obtained from the corresponding axisymmetric conjugate heat transfer case, is imposed at the wall interface. Having a fixed wall temperature profile is not expected to have a significant influence on the occurrence of flame asymmetries, since the time-scale of the wall is much larger than the reported time-scale of non-axisymmetric

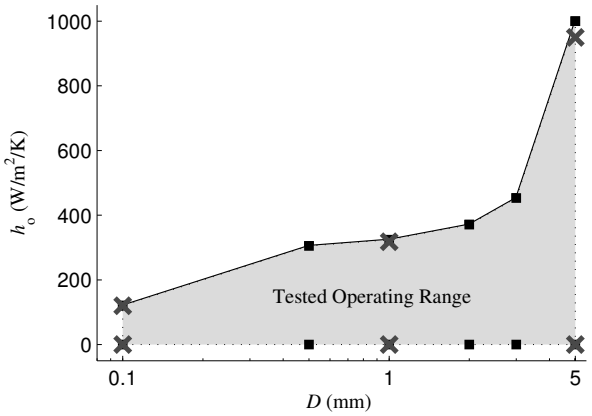

Figure 7: Range of tested operating conditions expressed in terms of external heat loss coefficient, h_o, and inner tube diameter, D. Conditions investigated using the axisymmetric assumption are contained within the shaded area bracketed by squares. 3-D simulations are performed at conditions corresponding to those shown with crosses.

flame cycles [52]. A parabolic velocity profile of average velocity S_{in}=10 m/s is set at the tube inlet. The stationary flames stabilized along the fixed wall temperature profile are very similar to those obtained with conjugate heat transfer, since the burning velocity of slowly-propagating excess-enthalpy flames, S_b, is almost equal to the inflow velocity, S_{in}.

Six different cases are simulated with fixed wall temperature profiles, both with the 2-D axisymmetric assumption, and in 3-D. These cases are chosen to bracket the wide range of tube diameters and heat loss conditions investigated in this study, as shown in Fig. 7. The 2-D grids cover a thin sector of the tube cross-section with only one cell in the circumferential direction. The 3-D grids cover the entire tube cross-section, and are based on an O-grid configuration, where the tube cross-section is divided by a centered inner square and 4 identical outer sections joining the outer square edges to the outer tube edge. Average spatial resolution is varied between 5 and 40 μm, which leads to 2-D grids with 1×10^4 to 3.9×10^4 elements, and 3-D grids with 3×10^5 to 7.2×10^6 elements, depending on tube diameter.

The 3-D solutions are initialized by interpolating the axisymmetric solution into the 3-D fluid grid. The cases are then simulated over a physical time twice as large as the residence time based on average flow velocity and simulation domain length. Since the grid geometry differs between 2-D and 3-D cases, the interpolation perturbs the solution slightly, which should be sufficient to trigger flame asymmetries [52]. Solutions for the largest diameter case, $D = 5.0$ mm, being the most likely to become asymmetric based on the concept of a critical diameter [23, 48, 49, 52], are additionally perturbed by re-initializing the velocity and pressure fields inside the fluid domain to a fixed uniform value. In all tested cases, the 3-D flames remain stable and axisymmetric, which justifies the use of the axisymmetric assumption for the range of conditions tested in this study. Given the differences in computational grids, the 2-D and 3-D results are essentially identical, as shown in Fig 8.

References

[1] S. Lloyd, F. Weinberg, A burner for mixtures of very low heat content, Nature 251 (1974) 47–49.

[2] D. Hardesty, F. Weinberg, Burners producing large excess enthalpies, Combust. Sci. Technol. 8 (1974) 201–14.

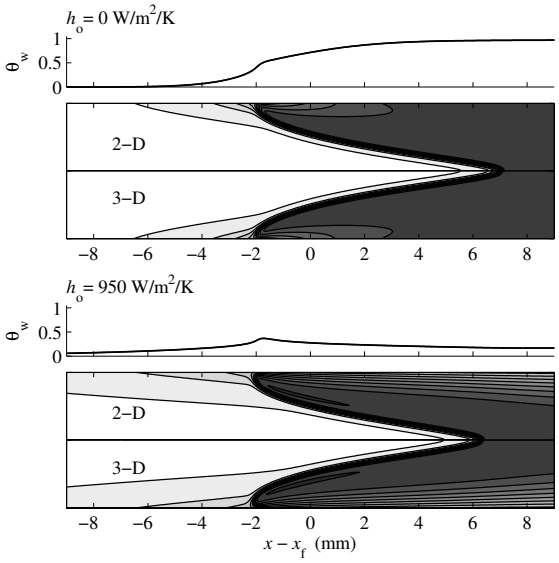

Figure 8: Contour plots of normalized fluid temperature, θ, obtained with both 2-D and 3-D models, for an inner tube diameter of $D = 5.0$ mm. Iso-contours are shown at intervals of 0.1 of θ. The wall temperature profile imposed at the wall interface, obtained from the conjugate heat transfer results at $h_o = 0$ W/m^2/K, and $h_o = 950$ W/m^2/K, respectively, are shown above the contour plots.

[3] N. Kaisare, D. Vlachos, A review on microcombustion: fundamentals, devices and applications, Prog. Energy Combust. Sci. 38 (2012) 321–359.

[4] T. Leach, C. Cadou, G. Jackson, Effect of structural conduction and heat loss on combustion in microchannels, Combust. Theor. Model. 10 (2006) 85–103.

[5] A. Gomez, J. Berry, S. Rouchoudhury, B. Coriton, J. Huth, From jet fuel to electric power using a mesoscale, efficient stirling cycle, Proc. Combust. Inst. 31 (2007) 3251–3259.

[6] J. Cho, C. Lin, C. Richards, R. Richards, J. Ahn, P. Ronney, Demonstration of an external combustion micro-heat engine, Proc. Combust. Inst. 32 (2009) 3099–3105.

[7] J. Bergthorson, M. Thomson, A review of the combustion and emissions properties of advanced transportation biofuels and their impact on existing and future engines, Renew. Sust. Energ. Rev. 42 (2015) 1393–1417.

[8] L. Sitzki, K. Borer, E. Schuster, P. Ronney, Combustion in microscale heat-recirculating burners, Third Asia-Pacific Conference on Combustion June 24-27 (2001).

[9] F. Weinberg, D. Rowe, G. Min, P. Ronney, On thermoelectric power conversion from heat recirculating combustion systems, Proc. Combust. Inst. 29 (2002) 941–947.

[10] H. Davy, Some new experiments and observations on the combustion of gaseous mixtures, with an account of a method of preserving a continued light in mixtures of inflammable gases and air without flame, Philos. Trans. R. Soc. Lond. 107 (1817) 77–85.

[11] D. Spalding, A theory of inflammability limits and flame-quenching, Proc. R. Soc. London Ser. A 240 (1957) 83–100.

[12] J. Buckmaster, The quenching of deflagration waves, Combust. Flame 26 (1976) 151–162.

[13] F. Williams, Combustion Theory, Benjamin Cummings, 1985.

[14] C. Hackert, J. Ellzey, O. Ezekoye, Effects of thermal boundary conditions on flame shape and quenching in ducts, Combust. Flame 112 (1998) 73–84.

[15] N. Kim, T. Kataoka, S. Maruyama, K. Maruta, Flammability limits of stationary flames in tubes at low pressure, Combust. Flame 141 (2005) 78–88.

[16] Y. Ju, K. Maruta, Microscale combustion: Technology development and fundamental research, Prog. Energy Combust. Sci. 37 (2011) 669–715.

[17] B. Lewis, G. von Elbe, Combustion, flames and explosions of gases, Elsevier Science, 2012.

[18] C. Chao, K. Hui, W. Kong, P. Chen, J. Wang, Analytical and experimental study of premixed methane-air flame propagation in narrow channels, Int. J. Heat Mass Transfer 50 (2007) 1302–1313.

[19] K. Kim, D. Lee, S. Kwon, Effects of thermal and chemical surface-flame interaction on flame quenching, Combust. Flame 146 (2006) 19–28.

[20] K. Maruta, T. Kataoka, N. Kim, S. Minaev, R. Fursenko, Characteristics of combustion in a narrow channel with a temperature gradient, Proc. Combust. Inst. 30 (2005) 2429–36.

[21] S. Lee, C. Tsai, Numerical investigation of steady laminar flame propagation in a circular tube, Combust. Flame 99 (1994) 484–490.

[22] N. Kim, K. Maruta, A numerical study on propagation of premixed flames in small tubes, Combust. Flame 146 (2006) 283–301.

[23] C. Tsai, The asymmetric behavior of steady laminar flame propagation in ducts, Combust. Sci. Technol. 180 (2008) 533–545.

[24] J. Daou, M. Matalon, Influence of conductive heat-losses on the propagation of premixed flames in channels, Combust. Flame 128 (2002) 321–339.

[25] C. Miesse, R. Masel, C. Jensen, M. Shannon, M. Short, Submillimiter-scale combustion, AIChE J. 50 (2004) 3206–3214.

[26] V. Zamashchikov, Experimental investigation of gas combustion regimes in narrow tubes, Combust. Flame 108 (1997) 357–359.

[27] V. Zamashchikov, An investigation of gas combustion in a narrow tube, Combust. Sci. Tech. 166 (2001) 1–14.

[28] V. Zamashchikov, S. Minaev, Limits of flame propagation in a narrow channel with gas filtration, Combust. Explo. Shock Waves 37 (2001) 21–26.

[29] Y. Ju, B. Xu, Theoretical and experimental studies on mesoscale flame propagation and extinction, Proc. Combust. Inst. 30 (2005) 2445–2453.

[30] Y. Ju, B. Xu, Effects of channel width and lewis number on the multiple flame regimes and propagation limits in mesoscale, Combust. Sci. Technol. 178 (2006) 1723–1753.

[31] D. Lee, K. Maruta, Heat recirculation effects on flame propagation and flame structure in a mesoscale tube, Combust. Theor. Model. 16 (2012) 507–536.

[32] G. Gauthier, G. Watson, J. Bergthorson, Burning rates and temperatures of flames in excess-enthalpy burners: A numerical study of flame propagation in small heat-recirculating tubes, Combust. Flame 161 (2014) 2348–2360.

[33] A. Jones, S. Lloyd, F. Weinberg, Combustion in heat exchangers, Proc. R. Soc. London Ser. A 360 (1978) 97–115.

[34] T. Takeno, K. Sato, K. Hase, An excess enthalpy flame theory, Proc. Combust. Inst. 18 (1981) 365–372.

[35] P. Ronney, Analysis of non-adiabatic heat-recirculating combustors, Combust. Flame 135 (2003) 421–439.

[36] D. Norton, D. Vlachos, Combustion characteristics and flame stability at the microscale: a CFD study of premixed methane/air mixtures, Chem. Eng. Science 58 (2003) 4871–4882.

[37] T. Leach, C. Cadou, The role of structural heat exchange and heat loss in the design of efficicent silicon micro-combustors, Proc. Combust. Inst. 30 (2005) 2437–2444.

[38] N. Kim, S. Kato, T. Kataoka, T. Yokomori, S. Maruyama, K. Fujimori, K. Maruta, Flame stabilization and emission of small swiss-roll combustors as heaters, Combust. Flame 141 (2005) 229–240.

[39] I. Schoegl, J. Ellzey, Superadiabatic combustion in conducting tubes and heat exchangers of finite length, Combust. Flame 151 (2007) 142–159.

[40] N. Kaisare, D. Vlachos, Optimal reactor dimensions for homogeneous combustion in small channels, Catalysis Today 120 (2007) 96–106.

[41] I. Schoegl, J. Ellzey, Numerical investigation of ultra-rich combustion in counter flow heat exchangers, Combust. Sci. Tech. 182 (2010) 1413–1428.

[42] V. Babkin, V. Drobyshevich, Y. M. Laevskii, S. Potytnyakov, Filtration combustion of gases, Combust. Explo. Shock Waves 19 (1983) 147–155.

[43] S. I. Potytnyakov, Y. M. Laevskii, V. S. Babkin, Effect of heat losses on propagation of stationary waves in filtration combustion of gases, Combust. Explo. Shock Waves 20 (1984) 15–22.

[44] Y. M. Laevskii, V. S. Babkin, V. I. Drobyshevich, S. I. Potytnyankov, Theory of filtrational combustion of gases, Combust. Explo. Shock Waves 20 (1984) 591–600.

[45] D. Norton, D. Vlachos, A CFD study of propane/air microflame stability, Combust. Flame 138 (2004) 97–107.

[46] G. Watson, J. Bergthorson, The effect of chemical energy release on heat transfer from flames in small channels, Combust. Flame 159 (2012) 1239–1252.

[47] C. Westbrook, F. Dryer, Simplified reaction mechanisms for the oxidation of hydrocarbon fuels in flames, Combust. Sci. Technol. 27 (1981) 31–43.

[48] V. Kurdyumov, G. Pizza, E. Fernandez-Tarrazo, Lewis number effect on the propagation of premixed laminar flames in narrow open ducts, Combust. Flame 128 (2002) 382–394.

[49] V. Kurdyumov, Lewis number effect on the propagation of premixed flames in narrow adiabatic channels: Symmetric and non-symmetric flames and their linear stability analysis, Combust. Flame 158 (2011) 1307–1317.

[50] G. Pizza, C. Frouzakis, J. Mantzaras, A. Tomboulides, K. Boulouchos, Dynamics of premixed hydrogen/air flames in microchannels, Combust. Flame 152 (2008) 433–450.

[51] G. Pizza, C. Frouzakis, J. Mantzaras, A. Tomboulides, K. Boulouchos, Dynamics of premixed hydrogen/air flames in mesoscale channels, Combust. Flame 155 (2008) 2–20.

[52] G. Pizza, C. Frouzakis, J. Mantzaras, A. Tomboulides, K. Boulouchos, Three-dimensional simulations of premixed hydrogen/air flames in microtubes, J. Fluid Mech. 658 (2010) 463–491.

[53] A. Bambrilla, M. Shultze, C. Frouzaki, J. Mantzaras, R. Bombach, K. Boulouchos, An experimental and numerical investigation of premixed syngas combustion dynamics in mesoscale channels with controlled wall temperature profiles, Proc. Combust. Inst. 35 (2015) 3429–3437.

[54] V. Zamashchikov, Some features of gas-flame propagation in narrow tubes, Combust. Explo. Shock Waves 40 (2004) 545–552.

[55] V. Kurdyumov, G. Pizza, C. Frouzakis, J. Mantzaras, Dynamics of premixed flames in a narrow channel with a step-wise wall temperature, Combust. Flame 156 (2009) 2190–2200.

[56] Y. Kotani, T. Takeno, An experimental study on stability and combustion characteristics of an excess enthalpy flame, Proc. Combust. Inst. 19 (1982) 1503–1509.

[57] Y. Kotani, H. Behbahani, T. Takeno, An excess enthalpy flame combustor for extended flow ranges, Proc. Combust. Inst. 20 (1984) 2025–2033.

[58] G. Gauthier, G. Watson, J. Bergthorson, An evaluation of numerical models for temperature-stabilized CH4/air flames in a small channel, Combust. Sci. Technol. 184 (2012) 850–868.

[59] F. Contarin, A. Saveliev, A. Fridman, L. Kennedy, A reciprocal flow filtration combustor with embedded heat exchangers: numerical study, Int. J. Heat Mass Transfer 46 (2003) 949–961.

[60] N. Kaisare, D. Vlachos, Extending the region of stable homogeneous micro-combustion through forced unsteady operation, Proc. Combust. Inst. 31 (2007) 3293–3300.